The 2015-2016 Study of wintertime PM$_{2.5}$ pollution in the Salt Lake Valley. Meteorological aspects and observations.

Sebastian W. Hoch
and Munkhbayar Baasandorj

Department of Atmospheric Sciences
135 S 1460 E, Rm 819
University of Utah
Salt Lake City, UT 84112-0110

Summary

Meteorological observations have been combined with detailed measurements of atmospheric chemistry during the persistent wintertime cold air pool and pollution episodes in the Salt Lake Valley during the 2015-2016-winter season. The goal of the study was to investigate the reactive pathways of the formation of the secondary aerosol ammonium nitrate, and to better understand links between atmospheric chemistry and meteorology.

While the valley heat deficit remains a good indicator for episodes of elevated $PM_{2.5}$ pollution, spatial and temporal variations of concentrations are caused by meteorological processes such as thermally-driven circulations (diurnal mountain winds and the lake breeze) and weak air-mass boundaries.

New findings include the identification of two production mechanisms of secondary particulate pollution (ammonium nitrate), one associated with the nighttime formation, the second with early-morning photochemical processes. Both are linked to the diurnal evolution of the basin meteorology. Further, a link is suggested between the effectiveness for the nighttime formation process of ammonium nitrate and the injection of clean, unpolluted, but oxidant-rich air along the basin sidewalls and through tributary canyons.

Table of Contents

1. Introduction

1.1 Background

The passing of high-pressure ridges during wintertime favors the formation of persistent wintertime cold air pools (PCAPs) in Utah's topographic basins. Under PCAP conditions, the boundary layer is stably stratified and/or capped by a capping inversion associated with warm-air advection aloft. Under these conditions, atmospheric mixing is limited and particulate pollutants and precursor gases emitted near the surface are accumulating, which often leads to the exceedance of the National Ambient Air Quality Standard (NAAQS) for $PM_{2.5}$. A typical winter in the Salt Lake City Basin sees about 6 multi-day events comprising 18 days when the NAAQS is exceeded (Whiteman et al. 2014).

1.2 Scope of Study

The Salt Lake Valley $PM_{2.5}$ Pollution Study was a multi-university study sponsored by the Utah Division of Air Quality. Researchers from the University of Utah (UU), Weber State University (WSU), Utah State University (USU), and from the Utah Division of Air Quality (DAQ) have combined their expertise and observational tools to study chemical transformation in Salt Lake Valley's persistent wintertime inversions. The goal of the study was to investigate the reactive pathways of the formation of secondary particulate pollutants and the coupling of meteorological and chemical processes.

1.3 Goals of this Report

This report covers the observations of meteorological conditions during the air pollution episodes of the 2015-2016 pollution season. Instrumentation ranging from small inexpensive temperature data loggers deployed along an elevation-transect from the valley floor up the basin sidewall, to sophisticated remote-sensing equipment such as ceilometers and a Doppler Wind LiDAR, were used to monitor the spatial and temporal variation of the atmospheric conditions within the valley cold air pools. This report documents the observations (location, instrumentation; Section 2), summarizes the meteorological analysis (Section 3), and highlights the key findings (Section 4).

2. Observations

The observational sites of the Salt Lake Valley $PM_{2.5}$ Pollution Study are shown on a map (**Fig. 1**) of the northeastern part of the Salt Lake Valley. The site names, abbreviations, elevations, type of measurements, and site coordinates are shown in Table 1. The key locations for chemistry and meteorological observations were Hawthorne Elementary (HW), the University of Utah William Browning Building (UU), the University of Utah Mountain Meteorology Laboratory at the mouth of Red Butte Canyon (RB), and the Neil Armstrong Academy (NAA). Radiosondes were launched twice a day by the National Weather Service (NWS) from the Salt Lake

International Airport (KSLC). Small and inexpensive temperature data loggers were distributed along an elevation transect running up the northeastern sidewall of the Salt Lake Valley. Additional *mobile* observation platforms were two instrumented TRAX trains and the KSL news helicopter.
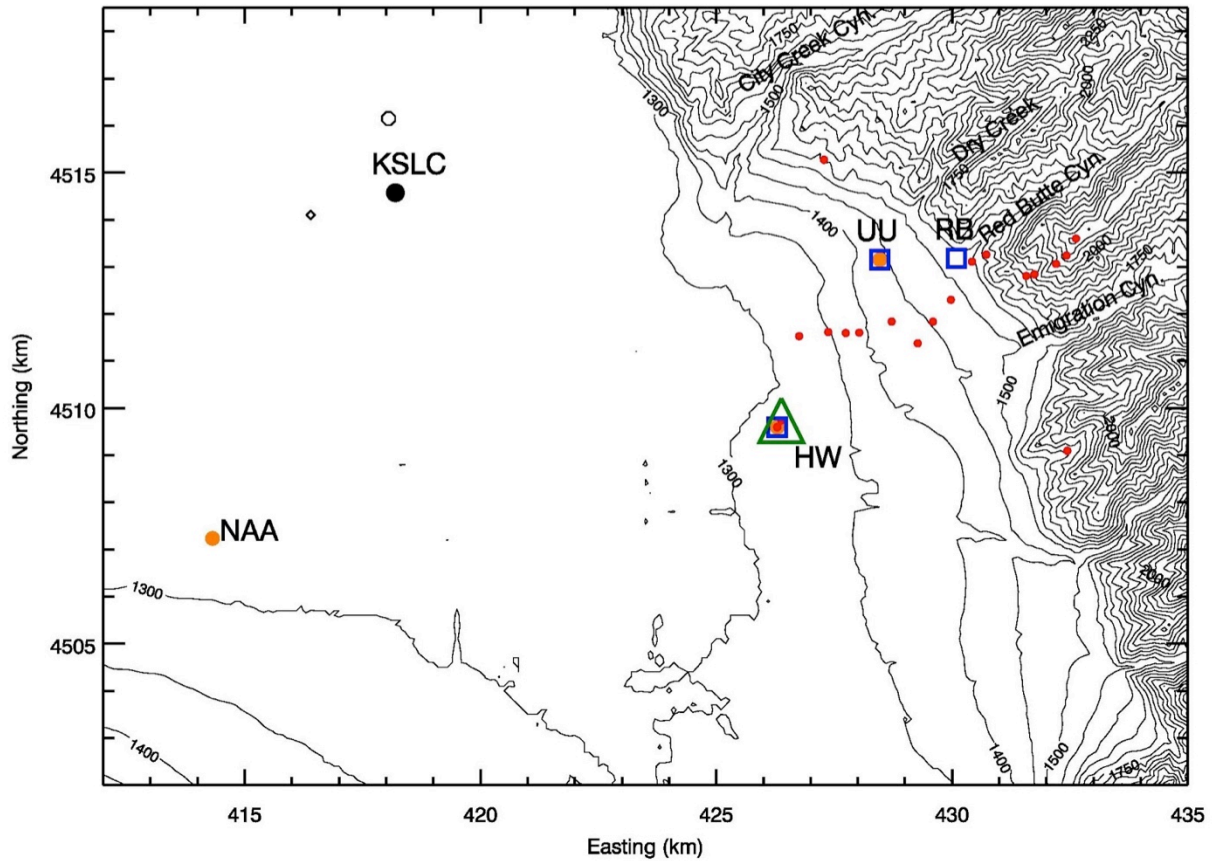
Figure 1: Map of the northeastern part of the Salt Lake City Basin (UTM projection, 50 m elevation contours), indicating the key location of the observational network. These include the sites with extended observations of chemistry (orange dots), Hawthorne Elementary (HW), the University of Utah William Browning Building (UU), the University of Utah Mountain Meteorology Laboratory at the mouth of Red Butte Canyon (RB), and the Neil Armstrong Academy (NAA). Locations with ceilometer measurements (blue squares), the UU Doppler Winds Lidar (green triangle), radiosonde location (black circle), and automatic temperature data loggers (red dots) are indicated.

Table 1: The main meteorological observational sites in the Salt Lake Valley.

Site Name	Site Abbreviation	Instrumentation	Elevation (m ASL)	Surrounding elevation (m ASL)	Elevation above ground (m)	Latitude (°N)	Longitude (°E)
University of Utah; William Browning Building	UU (base) and (top)	Temp/RH, Wind, Solar radiation, Turbulence, Ceilometer	1442 m 1465 m	1435 m	2 m and 30 m	40.766082° 40.766187°	-111.846752° -111.847718°
Hawthorne Elementary; UDAQ site	HW HW-LIDAR	Temp/RH, Wind, Turbulence, Ceilometer	1310 m	1308 m 1307 m	2 m 2 m	40.7343° 40.735269°	-111.8721° -111.871889°
Salt Lake City International Airport	KSLC	Temp/RH, Wind, Radiosonde	1289 m	1289 m	122 m	40.772436°	-111.954703°
Mountain Meteorology Laboratory; mouth of Red Butte Canyon	RB	Temp/RH, Wind, Ceilometer	1522 m	1520 m	2 m	40.7666°	-111.8284°
Neil Armstrong Academy	NAA	Temp/RH, Wind	1301 m	1298 m	3 m	40.71152°	-112.01448°

2.1 Temperature Profiles

Vertical profiles of the atmospheric temperature are necessary to evaluate static stability of the atmosphere and to help to define the strength of diurnal and persistent cold air pools. A good measure of the stability of a valley atmosphere is the Valley Heat Deficit (VHD, see **Section 3.1**). Two independent observations of the temperature structure in the Salt Lake Valley were made to calculate the VHD.

The first observation is readily available from the twice-daily radiosonde ascents from KSLC. Radiosondes are launched daily, at approximately 0500 and 1700 MST.

The second observation is based on a pseudo-vertical assumption (Whiteman and Hoch 2014), where temperature observations along an elevation transect are interpreted as a proxy for the vertical variation of temperatures within the valley or basin atmosphere. A set of 18 inexpensive temperature data loggers (Hobo Pro v2, Onset Computers, MA) was deployed housed in 6-plate radiation shields (R. M. Young, MI) along an elevation transect as indicated in **Fig.1**. **Table 2** lists the location of the sensors. With the exception of the topmost sensor, they were deployed at a height of approximately 130 to 180 cm above the surface. Sensors in the upper basin were installed on available dead branches of the vegetation, to avoid any disturbance of the environment. See **Figure 2** for example deployments. The topmost sensor on the summit of Mt. Wire was installed on the top of a freely accessible tower, approximately 10 m AGL. Temperature data was recorded every 5 minutes and stored on local memory.

Table 2: Locations of HoboPro® automatic data loggers used to calculate the pseudo-vertical temperature profile in the Salt Lake Valley.

#	Latitude [°N]	Longitude [°E]	Elevation [m ASL]	Description
1	40.73528	-111.87189	1307	Wim's back yard
2	40.73398	-111.87291	1308	HW-1
3	40.73398	-111.87291	1308	HW-2
4	40.75146	-111.86762	1311	8th & 8th
5	40.75231	-111.86035	1338	Ed's house
6	40.75216	-111.85593	1372	Ryan's buddy's house
7	40.75225	-111.85254	1388	Baptist Church
8	40.75443	-111.84443	1428	Steiner Center
9	40.75032	-111.83782	1429	Judy's house
10	40.75449	-111.83406	1453	Corner Bakery
11	40.75868	-111.82959	1481	Marriott
12	40.76602	-111.82439	1541	Red Butte (lower)
13	40.7674	-111.82082	1622	Red Butte (upper)
14	40.76339	-111.81072	1737	Mt Wire - 1 - lower basin
15	40.76371	-111.80868	1822	Mt Wire - 2 - ridge a
16	40.76573	-111.80326	2000	Mt Wire - 3 - ridge b
17	40.76736	-111.80067	2084	Mt Wire - 4 - ridge c
18	40.77061	-111.79833	2170	Mt Wire - 5 - top tower
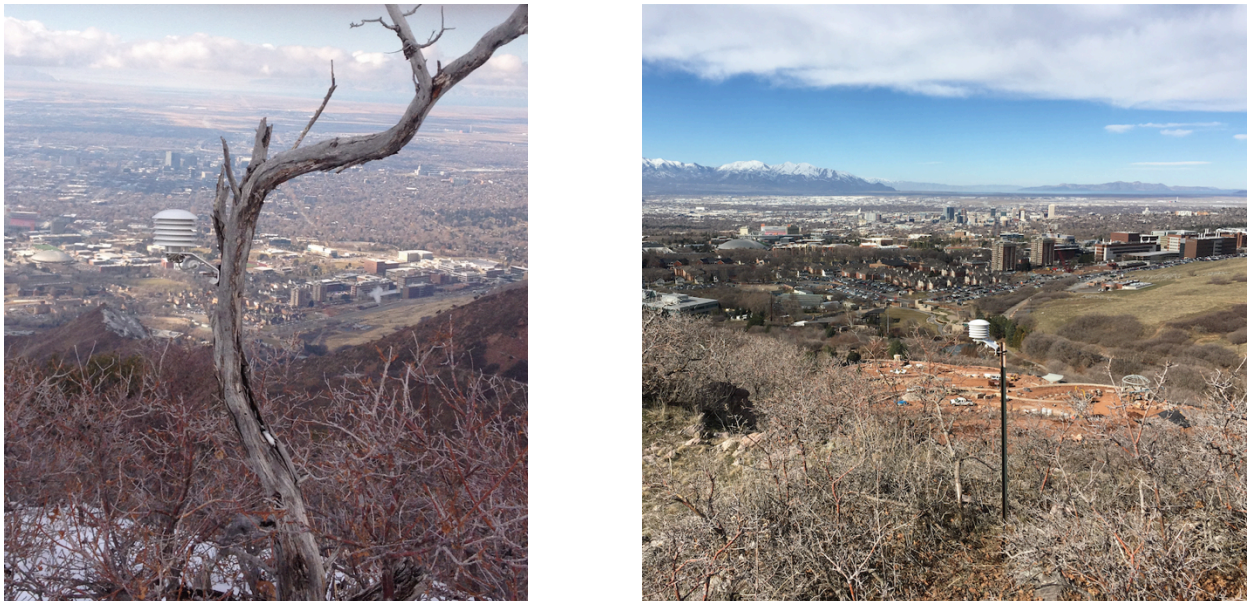
Figure 2: Example deployments of HoboPro® automatic data loggers on the ridge of Mt. Wire (#16) and in the upper part of Red Butte Gardens (#13).

2.2   Wind Profiles

Wind profiles, while available from the twice-daily radiosondes from KSLC (see **Section 2.1**) were continuously recorded using the University of Utah Halo Photonics Doppler wind lidar (**Fig. 3**). The lidar was installed in a backyard of a local volunteer who lives in the direct vicinity of Hawthorne Elementary (HW) site. The installation required a fixed power source and an

unobstructed view of sky. The lidar was programmed to scan a Plan Position Indicator (PPI) scan pattern every 10 minutes. The Vertical Azimuth Display (VAD) analysis was used to retrieve the vertical profile of the three-dimensional wind field. This wind field can be overlaid with the aerosol backscatter coefficient of the lidar retrieval or of the co-located ceilometer (see **Section 2.3**). Daily quicklooks (see **Fig. 4** for an example) were produced during the experiment and shared via a web page with the collaborators and interested public.

Figure 3: The University of Utah Halo Photonics Streamline Doppler Wind Lidar deployed during the Salt Lake Valley PM$_{2.5}$ Pollution Study near the HW site.
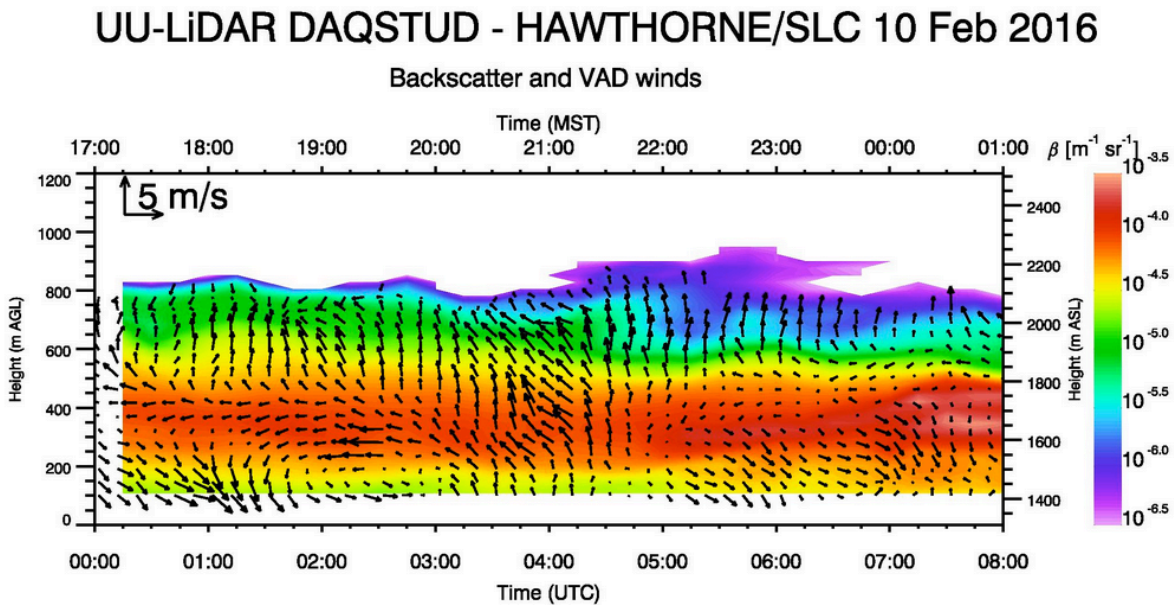
Figure 4: Example quicklook product (subset) showing the Doppler wind lidar retrieved vertical profile of the wind field above the Hawthorne (HW) site.

2.3   Aerosol Backscatter

Aerosol backscatter profiles were recorded at three locations in the Salt Lake Valley to resolve spatial differences in the atmospheric pollution loading and to resolve temporal changes in the aerosol optical properties at these three sites. Ceilometers (Vaisala CL31), as depicted in **Figure 5**, were deployed at the Hawthorne (HW), University of Utah (UU), and Red Butte Canyon Exit (RB) sites.

Figure 5: One of the three Vaisala CL31 ceilometers deployed during the Salt Lake Valley PM$_{2.5}$ Pollution Study (UU site shown).

The instruments recorded a vertical profile (10-m resolution) of the atmospheric aerosol backscatter coefficient β every 16 seconds. The raw data was averaged to 10-min means for further processing. Daily quicklooks were made available daily during the experiment via a website. An example is shown in **Figure 6**. One scientific goal was to investigate the relationship between surface observations of PM$_{2.5}$ concentrations and the aerosol backscatter coefficient β of the near-surface air layers. See **Section 3.2** for more detail.

Time-height cross sections of aerosol backscatter illustrate changes in the polluted PCAP atmosphere, and visualize mixing processes, layering, and injection of clean air along basin sidewalls or through tributary canyons. Further, phases of quickly intensifying backscatter retrievals seem to indicate periods of PM$_{2.5}$ formation.
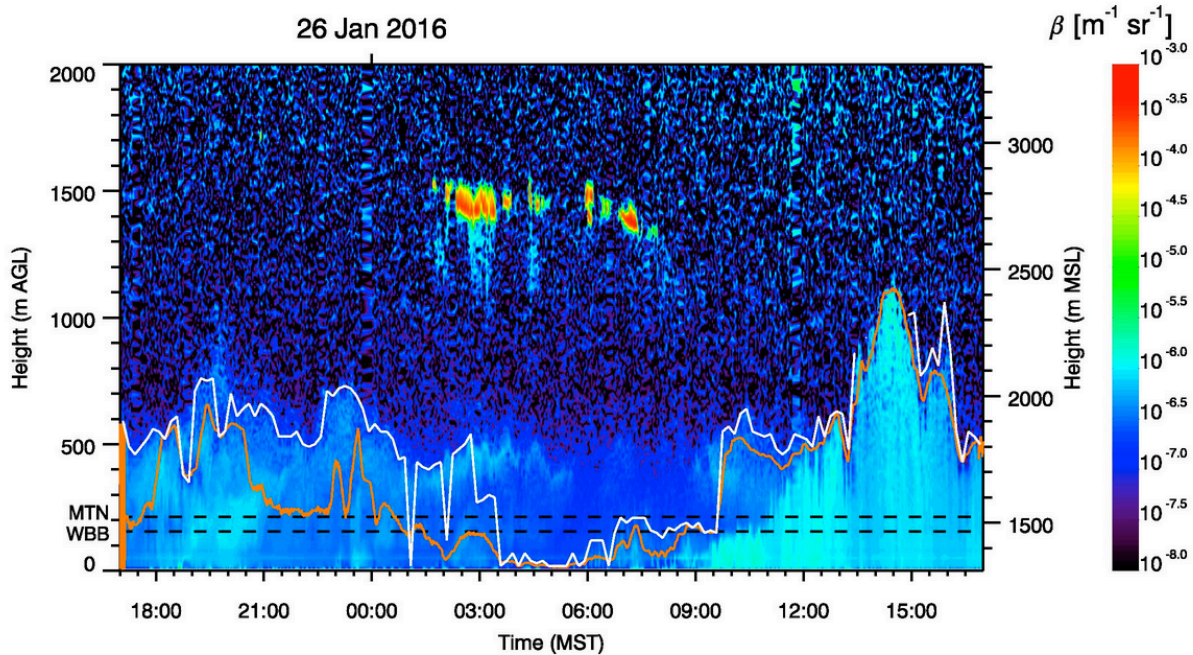
Figure 6: Example quicklook product showing the ceilometer retrieved vertical profile of the aerosol backscatter coefficient (β) at the Hawthorne (HW) site. The white and orange lines represent two different estimates of atmospheric mixing heights.

2.4   Turbulence Intensity and Vertical Mixing

Turbulence kinetic energy (TKE) is a measure of turbulence intensity. To evaluate the strength of atmospheric mixing at the valley sidewall (UU) and valley floor (HW) locations, turbulence observations were made using Campbell Scientific CSAT3 ultrasonic anemometers (UU rooftop site) and an EC150 open path gas analyzer (HW site) to measure the three-dimensional wind field and vertical temperature, humidity and CO_2 fluctuations at 20 Hz. This dataset was processed using the Utah Turbulence in Environmental Studies processing and analysis code (UTESpac). **Figure 7** shows the instrumentation.

A second measure of atmospheric mixing and turbulence is the vertical velocity variance (σ_w) that was derived from vertical stare data collected with the University of Utah Doppler wind lidar.

Figure 7:   Turbulence observations with an EC150 open-path gas analyzer at the Hawthorne (HW) site (left) and a CSAT3 sonic anemometer at the University of Utah (UU) rooftop location (right).

2.5   Solar and Infrared Radiation

Solar radiation was measured at the University of Utah (UU) site. Incoming solar radiation was measured with a pyranometer (CMP21, Kipp and Zonen, Delft, the Netherlands) on the roof of the William Browning Building (WBB). Reflected solar radiation was measured at 1.3 m AGL on a lawn outside WBB using photodiode-type pyranometer (SP-110, Apogee, Logan UT). Observations of solar radiation can indicate the degree of cloudiness and the amount of

radiative energy available to drive photochemical reactions. The surface albedo - the ratio between reflected solar and incoming solar radiation - indicates the surface conditions such as the degree snow cover or bare grass surface.

Further, longwave (infrared) incoming radiation was measured on the rooftop (WBB) location. Changes in infrared incoming radiation indicate the degree of cloud cover and cloud height. **Figure 8** shows the instrumentation deployed at the UU locations.

Figure 8:   Radiation measurements at the University of Utah (UU) rooftop (left) and lawn (right) sites.

2.6   Basic Weather Observations

Basic weather observations (temperature and relative humidity, pressure, wind speed and direction) are available for many location throughout the Salt Lake Valley via MesoWest (Horel et al. 2002; see mesowest.utah.edu), and could be retrieved for the Neil Armstrong Academy (NAA), University of Utah rooftop (UU), Red Butte Canyon Exit (RB), etc. Basic meteorological data in high temporal resolution from Hawthorne (HW) was received from Utah Division of Air Quality. One additional automatic weather station was installed on a lawn surface east of the UU rooftop site (see **Fig. 8**). This dataset was used to evaluate the temperature stratification on the UU sidewall site and to look for signs of nocturnal downslope flows influencing the chemical composition of the valley sidewall atmosphere.

Computer code was written to ingest any MesoWest weather observation via an API query to the meteorological dataset and to produce daily quicklooks to evaluate weather conditions within the Salt Lake Valley. **Figure 9** shows an example of a daily quicklook product.
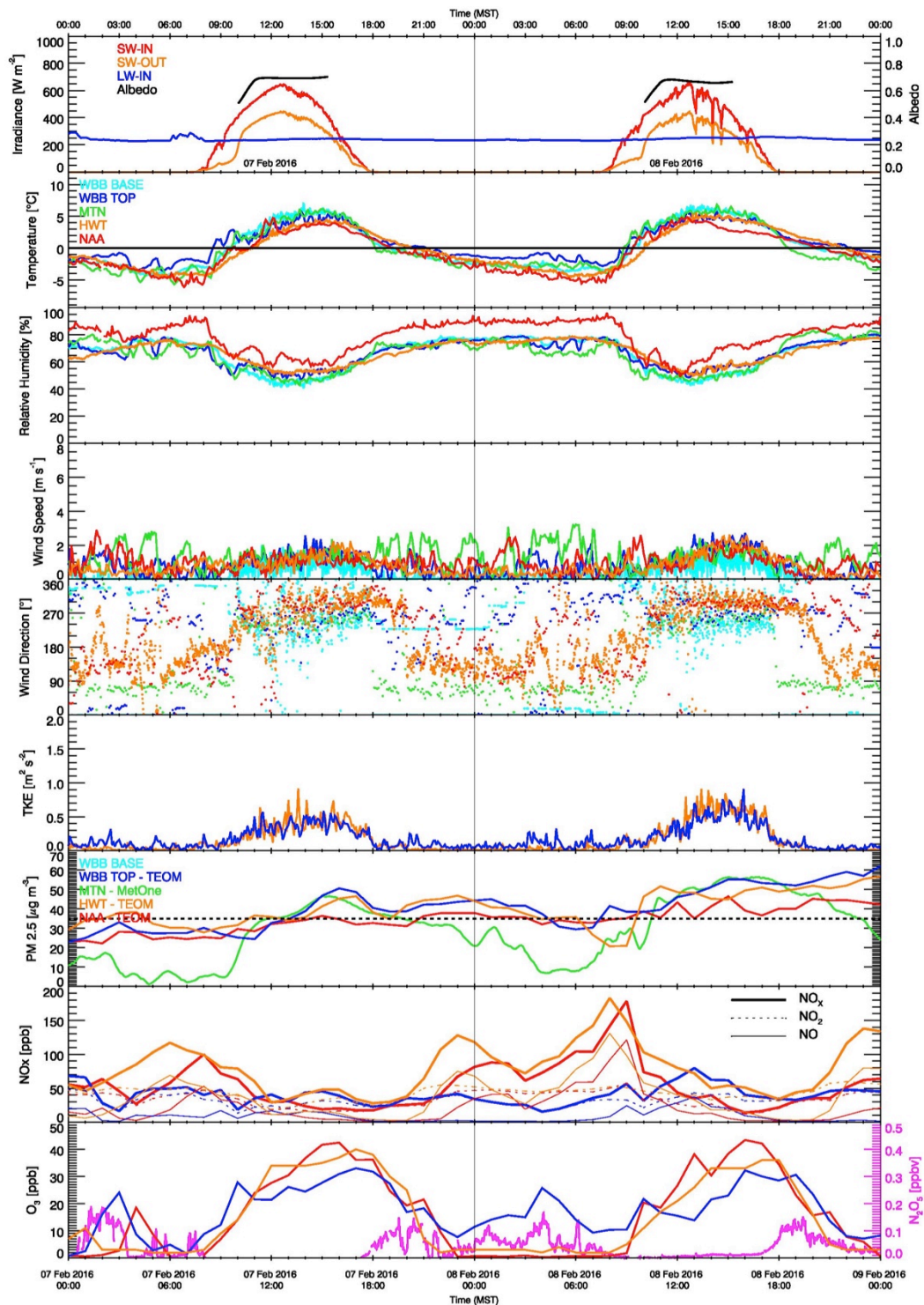
Figure 9: Example quicklook product showing meteorological and chemical observations as a 2-day time series. Variables shown are solar in- and outgoing and incoming longwave radiation, albedo, temperature, relative humidity, wind speed, wind direction, turbulence kinetic energy, PM$_{2.5}$, NO$_X$, and O$_3$ and N$_2$O$_5$ concentrations.

2.6   Mobile observation platforms

Besides the surface-based and remote sensing platforms, two datasets from mobile platforms were available during the experiment. These were deployed and maintained by unfunded collaborators who were willing to share their datasets. The mobile platforms consisted of two TRAX trains operated by the Utah Transit Authority (UTA) and the local news helicopter operated by KSL, and were equipped with $PM_{2.5}$ concentration monitors.

3. Meteorological Analysis

3.1   Vertical Temperature Structure and Valley Heat Deficit

The valley heat deficit (VHD) is a measurement of the amount of energy that would be needed to bring a valley or basin atmosphere to a neutral stratification. Following Whiteman et al. (1999, 2014) it is calculated for the Salt Lake Valley as

$$VHD = c_p \int_{1300\,m}^{2200\,m} \rho(z)\,[\theta_h - \theta(z)]\;dz, \quad [\mathrm{J\ m^{-2}}]$$

where θ_h is the potential temperature at height h, $\rho(z)$ and $\theta(z)$ are the air density and potential temperature from the twice-daily rawinsonde sounding, respectively. The specific heat of air at constant pressure is denoted as c_p, and dz is 10 m. The VHD is the heat required to warm an atmospheric column with a 1-m^2 base to the potential temperature observed at the top of the basin at height $h=2200\,m$, bringing the underlying atmosphere to a dry adiabatic lapse rate. Calculations were performed using the twice-daily radiosondes launched by the National Weather Service (NWS) at the KSLC site and based on the pseudo-vertical temperature soundings recorded along the northeastern valley sidewall. For the Salt Lake Valley, the elevation range between 1300 m ASL (valley floor) and the height of 2200 m, corresponding the mean ridge height surrounding the valley, are used. Calculations of VHD reveal the episodes of high atmospheric stability during the passage of high-pressure centers across Northern Utah.

The upper panel of **Figure 10** shows the time series of potential temperatures at the valley floor (~1300 m MSL) and at the mean top height of the Salt Lake City Basin, ~2200 m MSL, derived from radiosonde observations by the National Weather Service from the Salt Lake City Airport. The difference between the two curves indicates the bulk stability of the valley atmosphere. When the two curves touch, the atmosphere is referred to as neutral for dry adiabatic processes and there is no resistance to vertical mixing. The further the two curves deviate, the higher is the stability and the harder it is to mix pollutants emitted at the surface. These time series further illustrate that the strong wintertime cold pool episodes are often caused by warm air advection aloft rather than through enhanced cooling near the surface. The bottom panel of **Figure 10** shows the VHD together with smoothed $PM_{2.5}$ pollution concentrations (red curve). The good correlation between VHD and $PM_{2.5}$ becomes evident, and has previously been reported by Whiteman et al. (2014).

Persistent cold air pools or PCAPs can be defined as periods when the VHD exceeds a threshold value of 4.04 MJ m^{-3} (Whiteman et al. 2014). In the Salt Lake Valley, this VHD threshold value corresponds PM$_{2.5}$ concentrations of 17.5 µg m^{-3}, which is half of the NAAQS for PM$_{2.5}$. After a VHD value of 4.04 MJ m^{-3} is reached, pollution concentrations tend to increase monotonically at a rate of approximately 10 µg m^{-3} day^{-1} (Whiteman et al. 2014).
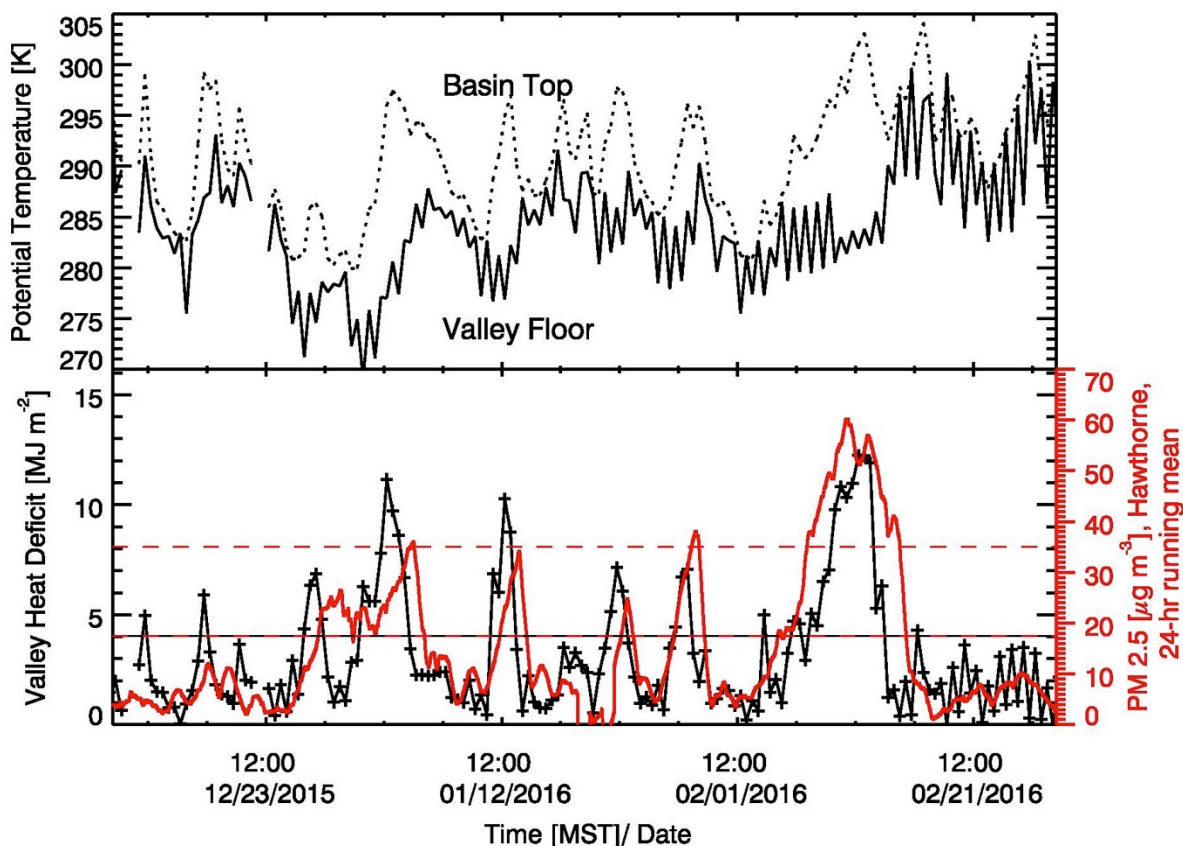
Figure 10: Potential temperature at the base and top of the Salt Lake City Basin from radiosonde observations by the National Weather Service (top), and the Valley Heat Deficit (VHD, black) and the smoothed observations of PM$_{2.5}$ pollutant concentrations (red) from the UDAQ Hawthorne (HW) site. Data covers the main observational period of the experiment, from 10 December 2015 through 28 February 2016. Note that the horizontal dashed line marks the NAAQS for PM$_{2.5}$ and the horizontal red-black dashed line marks the VHD threshold value of 4.04 MJ m^{-3} and a PM$_{2.5}$ concentrations of 17.5 µg m^{-3}.

Following this definition, there were 6 PCAP episodes in 2015-2016 winter season, as summarized in **Table 3**. Four of these episodes were rather short and lasted not longer than 48 hours. During these episodes, the pollution levels did not exceed the 24-hour NAAQS for PM$_{2.5}$. During the longer-lived episodes in early January and early-mid February, the NAAQS was exceeded once and eight times, respectively. Typically, an increase in VHD is followed by an increase in PM$_{2.5}$ concentrations, as seen in the first 5 of the 6 episodes. In the beginning of episode #6, a rapid increase in the PM$_{2.5}$ concentration is seen early on, while the VHD hovers

around the threshold value for a PCAP. Yet another interesting feature in the 2015-2016 winter is the connection between the 1st and 2nd PCAP periods. Particulate pollution concentrations remain elevated following PCAP #1 and increase continuously from this elevated level when PCAP conditions settle back in after three days. There are different hypothesis that could be investigated, involving near-surface stable layers or the boundary layer of the Great Salt Lake that could act as pollution reservoirs for accumulated pollutants. These hypotheses deserve further investigation if funding for additional analysis becomes available.

Table 3: Summary of persistent cold air pool (PCAP) episodes during the 2015-2016 winter season, defined by valley heat deficit values above 4.04 MJ m^{-3}.

#	Start	End	# 12-hour VHD values > 4.04 MJ m^{-3}	Maximum VHD [MJ m^{-3}]	# PM$_{2.5}$ NAAQS exceedences
1	12/27/2015 0500 MST	12/23/2015 1700 MST	4	6.85	-
2	01/01/2016 0500 MST	01/04/2016 1700 MST	8	11.16	1 x (4 Jan. 2016)
3	01/12/2016 0500 MST	01/13/2016 1700 MST	4	10.26	-
4	01/22/2016 0500 MST	01/23/2016 0500 MST	3	7.17	-
5	01/27/2016 1700 MST	01/28/2016 1700 MST	3	7.07	-
6	02/08/2016 0500 MST	02/14/2016 0500 MST	13	12.25	8 x (7-14 Feb.2016)

For the first time, the VHD was calculated from a pseudo-vertical temperature profile dataset. There are certain limitation of the pseudo-vertical assumption, as detailed in Whiteman and Hoch (2014). The key problems arise as the temperature sensors are affected by the surface layer along the terrain cross-section. During nighttime (daytime), pseudo-vertical sounding profiles tend to be colder (warmer) than the approximated valley atmosphere, as the measurements along the sidewall are made within a stable (unstable) near-surface layer. Calculations on the VHD using pseudo-vertical observation will further be affected by spatial differences in these surface layer effect among the individual along-slope observations, and the observation sites should be chosen to minimize these effects by avoiding microclimates along the terrain cross section.

A comparison among the retrievals of the VHD via the radiosondes and the pseudo-vertical profiles based on the "Hobo-Lines" (named after the thermometer model name, "HoboPro") shows differences arising from the caveats discussed above. **Figure 11** shows time series of both VHD retrievals for the longest pollution event of the 2015-1016 winter season (top panel) and for the entire winter season. **Figure 12** shows a scatter plot illustrating the correlation between the two retrieval methods based on the radiosondes and the pseudo-vertical soundings. The linear Pearson correlation coefficients are 0.64, 0.60 and 0.67 for all times, daytime, and nighttime, respectively.
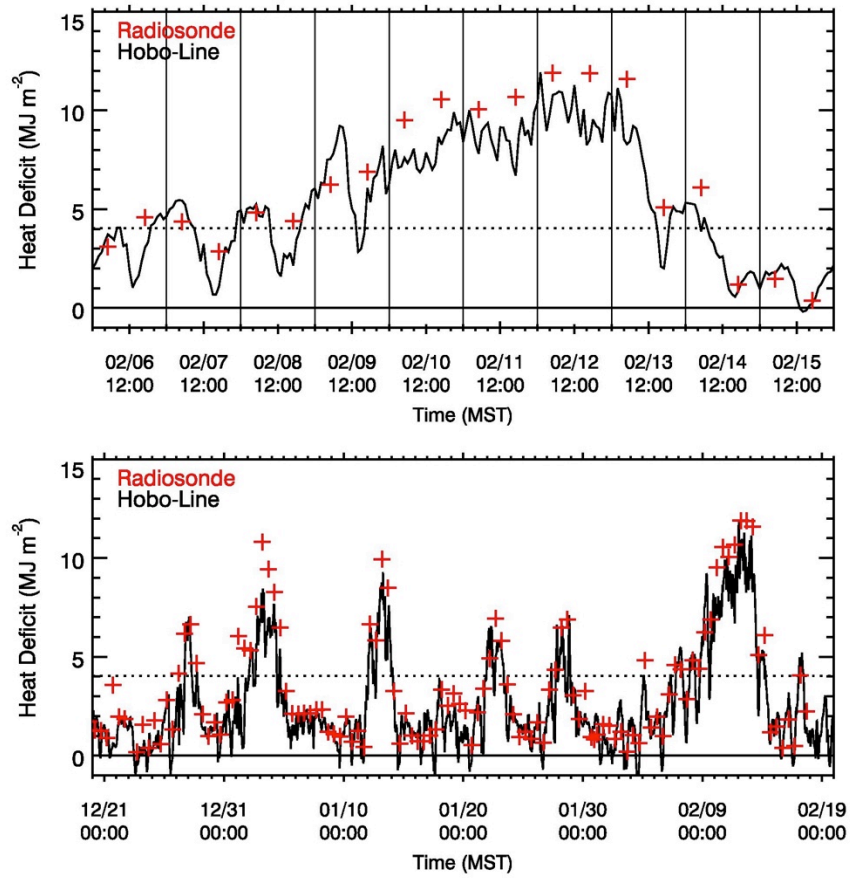
Figure 11: Time series of Valley Heat Deficit (VHD) calculations based on twice-daily radiosondes (red) and from the continuously available pseudo-vertical temperature profile measured with inexpensive "Hobo" data loggers (black), for the longest pollution episode during (top panel), and the entire 2015-2016 winter season (bottom panel).
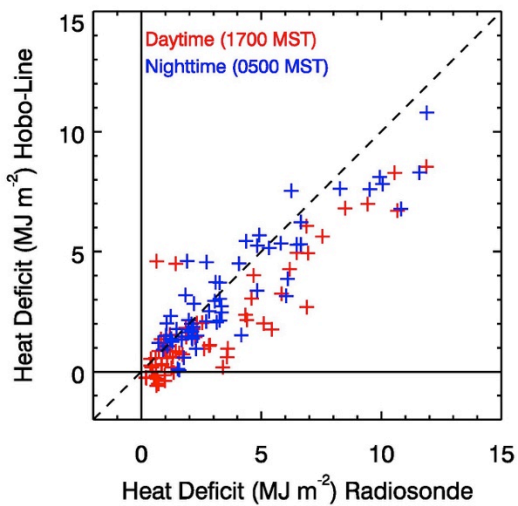
Figure 12: Scatterplot between the daytime (1700 MST, red) and nighttime (0500 MST, blue) retrievals of the Valley Heat Deficit (VHD) based on the twice-daily radiosonde ascents at KSLC and calculated from the pseudo-vertical temperature soundings based on an elevation transect with inexpensive "Hobo" temperature data loggers.

A different way to visualize the thermal stratification and to identify atmospheric stable layers are time-height cross sections of potential temperatures. **Figure 13** gives an overview over the entire 2015-2016 winter season. In addition to the isentropes (contours of constant potential temperature), regions with elevated atmospheric stability ($d\theta/dz > 0.016$ K m^{-1}) are highlighted in red. The formation of capping inversions associated with warm air advection aloft and the effect of nocturnal near-surface cooling are well illustrated.
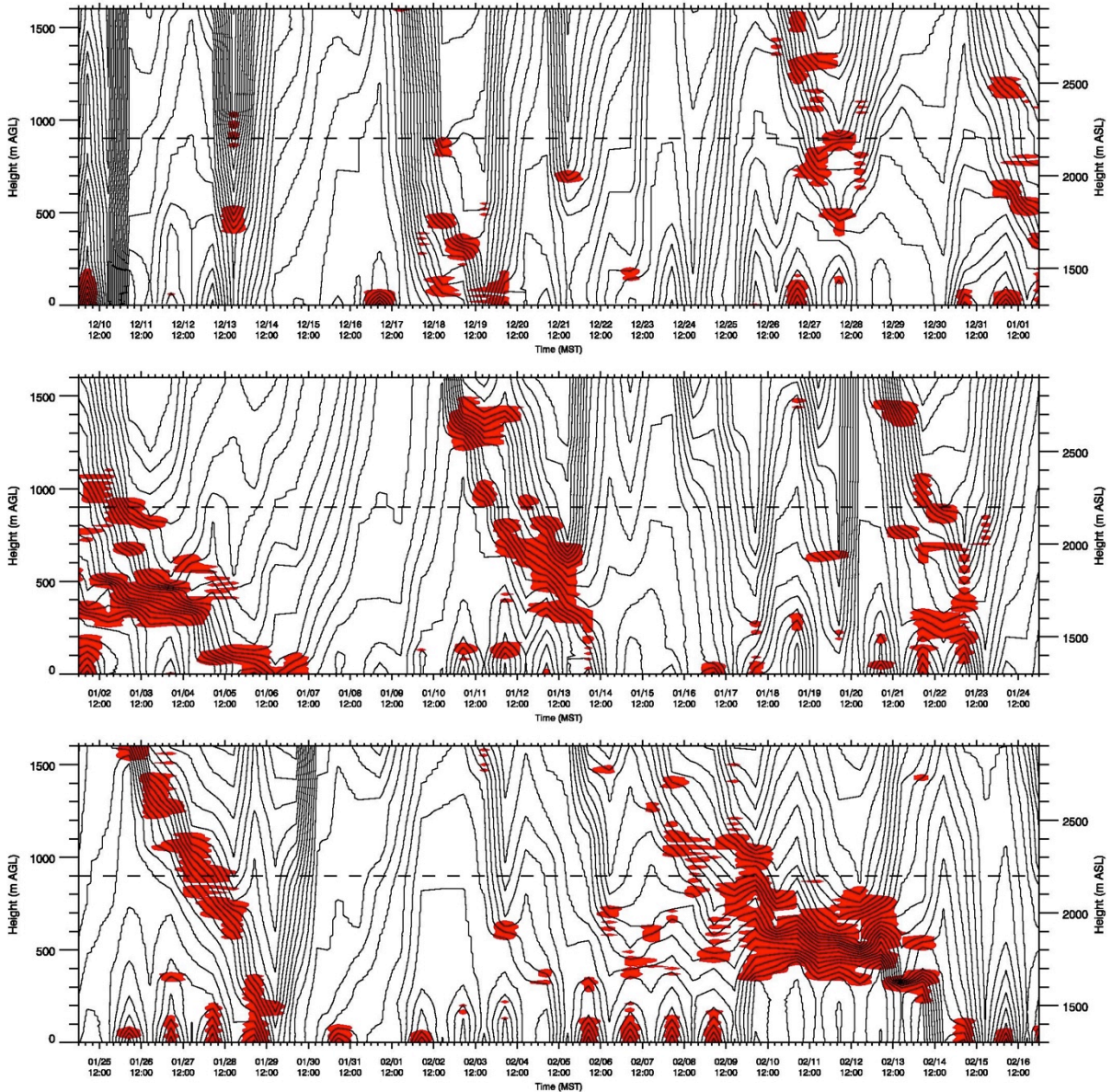
Figure 13: Time-height cross-section of *insentropes* (isolines of constant potential temperature θ) as recorded by twice-daily radiosondes at KSLC during the experimental winter season. Regions with elevated atmospheric stability ($d\theta/dz > 0.016$ K m^{-1}) are highlighted in red.

Changes in the diurnal evolution of the vertical temperature structure are not only observed between days within or outside pollution episodes, but also within pollution episodes. Typically, a PCAP forms under clear-sky conditions, but moisture accumulates over time and a fog-filled, or stratus-topped PCAP develops.
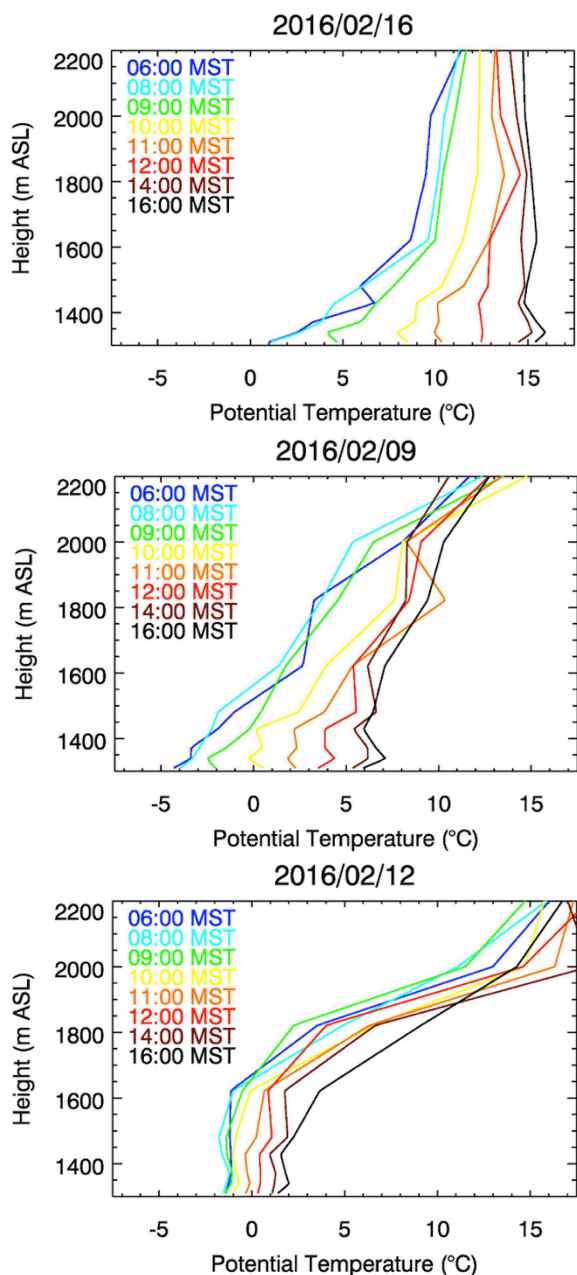
Figure 14: Pseudo-vertical potential temperature profiles during selected times of three days that characterize a clear, unpolluted day (top, 16 Feb. 2016), a clear-sky PCAP (middle, 9 Feb. 2016), and a foggy PCAP (bottom, 12 Feb. 2016).

Figure 14 shows selected pseudo-vertical profiles of potential temperature for selected times during three days that represent clear, unpolluted conditions (top, 16 Feb. 2016), PCAP conditions during the start of the 6-16 Feb. PCAP when skies were mostly clear (middle, 9 Feb. 2016), and the midst of the fog filled, stratus-capped, later part of the 6-16 Feb. PCAP (bottom). During unpolluted conditions, a temperature cycle with a large diurnal amplitude, especially near the surface, is seen. Conditions are very (statically) stable at night, with a strong inversion in the lowest 300 m. During the day, however, the inversion is broken up as a convective boundary layer forms near the surface, and the entire basin atmosphere reaches a dry-adiabatic lapse rate by early afternoon. During PCAP conditions, on the other hand, the surface heating is not sufficient for a convective layer to extend to the cold-air pool top. The atmosphere remains stably stratified and pollutants and precursor gases stay trapped. Under cloud-topped conditions in a mature stage of a PCAP, yet a different temperature structure arises. The amplitude of the diurnal temperature cycle is greatly reduced, and a well-mixed layer in the lowest few hundred meters is capped by a strong capping inversion. Cloud-top cooling is likely playing an important role in producing cold air at the inversion top, which leads to a top-down convection in the lowest, near-surface layers. This likely leads to a more homogeneous distribution of pollutants within the PCAP throughout the full diurnal cycle. A strong stratification along the basin sidewalls may reduce the penetration depth of nighttime down-canyon flows, limiting both clean-air advection and the injection of oxidants from air above the PCAP.

3.2 PM$_{2.5}$ concentration and aerosol backscatter

One of the scientific goals was to investigate the relationship between aerosol backscatter retrievals from the deployed Vaisala CL31 ceilometers and surface values of co-located PM$_{2.5}$ concentrations. For this endeavor, backscatter values from ~40 m AGL at Hawthorne were compared to the average surface PM$_{2.5}$ concentrations reported at that site. Correlations were calculated between both PM$_{2.5}$ and PM$_{10}$ concentrations and the aerosol backscatter coefficient β. A strong dependence of these relationships were found for different levels of atmospheric moisture (relative humidity). This is likely due to that fact that a liquid film can form around hygroscopic aerosol, which leads to a higher backscatter.

An example correlation between and PM$_{10}$ concentrations with the aerosol backscatter coefficient β for a relative humidity between 55% and 60% is shown in **Figure 15**. **Figure 16** shows the variation of the slope of the linear fit between both PM$_{2.5}$ and PM$_{10}$ concentrations with the aerosol backscatter coefficient β. This illustrates that a stronger dependence on relative humidity results if the backscatter is related to PM$_{10}$ concentrations, while the backscatter values interpreted as a linear function of PM$_{2.5}$ concentrations shows a weaker dependence.
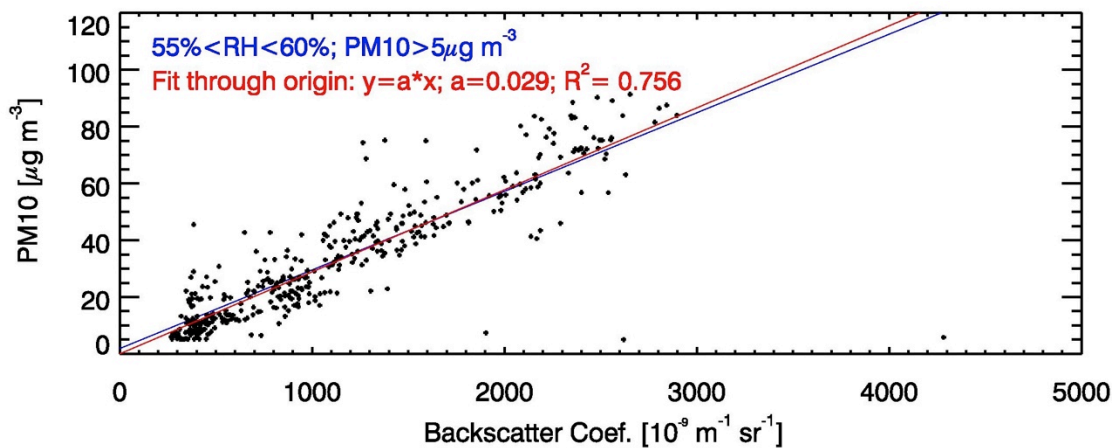
Figure 15: Scatterplot illustrating the linear relationship between PM$_{10}$ concentrations and the ceilometer-derived aerosol backscatter coefficient β, in this case for relative humidity levels between 55% and 60%. A linear fit through the origin is used to calculate the slope of this relationship and a correlation coefficient.

Further steps were undertaken to use these relationships to test the predictability of particulate concentrations - both PM$_{2.5}$ and PM$_{10}$ - from ceilometer-derived aerosol backscatter values. Preliminary results were mixed, as predicted levels could vary by more 100%. Further refinement of this methodology is needed and other factors, such as the vertical variation in relative humidity, variations in observed size distributions, and a dependence on dominating chemical composition need to be evaluated.
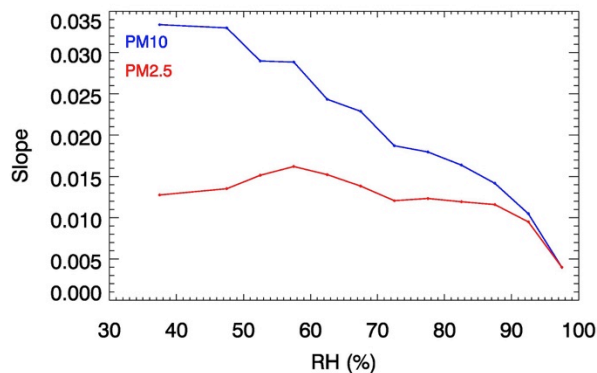
Figure 16: The slope (in units of 10^{-9} m^{-1} sr^{-1} μg^{-1} m^3) of the linear relationship between $PM_{2.5}$ (red) and PM_{10} (blue) concentrations with the ceilometer-derived aerosol backscatter coefficient β as a function of relative humidity (RH [%]). A stronger dependence is seen for PM_{10} than for $PM_{2.5}$ estimates.

4. Key Findings

4.1 Spatial and Temporal Variations of $PM_{2.5}$ concentrations

Daily mean 24-hour $PM_{2.5}$ concentrations observed at HW, UU and NAA do not show very large differences over the course of the experimental period, as shown in **Figure 17**. This indicates that on the time scale of days, $PM_{2.5}$ pollution is distributed fairly homogeneously. When pollutant levels are high, HW readings are typically slightly more elevated compared to the levels at UU and NAA. For example, during days when HW levels exceed 17.5 μg m^{-3}, levels are 4 μg m^{-3} and 2.5 μg m^{-3} lower at the UU and NAA sites. Interestingly, levels at NAA are typically higher (by 2 μg m^{-3}) during days when HW readings are below 10 μg m^{-3}. These values are just indications of small spatial differences and more data would be necessary for a proper statistical analysis.

However, on timescales smaller than 24-hours, and over spatial scales extending to different topographic basins in northern Utah, differences in $PM_{2.5}$ concentrations could be detected. These differences, of which a selection is discussed below, are connected to meteorological processes.

Figure 17: 24-hour average $PM_{2.5}$ concentrations (top panel) observed at the three study sites, UU (red), HW (blue) and NAA (black) during the 2015-2016 winter season. Data are from TEOM measurements. Differences in 24-hour concentrations from the HW value are shown in the bottom panel.

19

Horizontal variations

The morning distribution of PM$_{2.5}$ pollution in the Salt Lake Valley on 8 February showed a remarkable variation. A strong gradient of concentrations was observed at 10 MST along the north-south TRAX transect, as shown in **Figure 18**. Concentrations above (below) 35 µg m^{-3}, dominate in the northern (southern) part of valley as shown by red (yellow) colors. Also, note the even lower concentration recorded near the mouth of Red Butte Canyon (green, 10 µg m^{-3}).
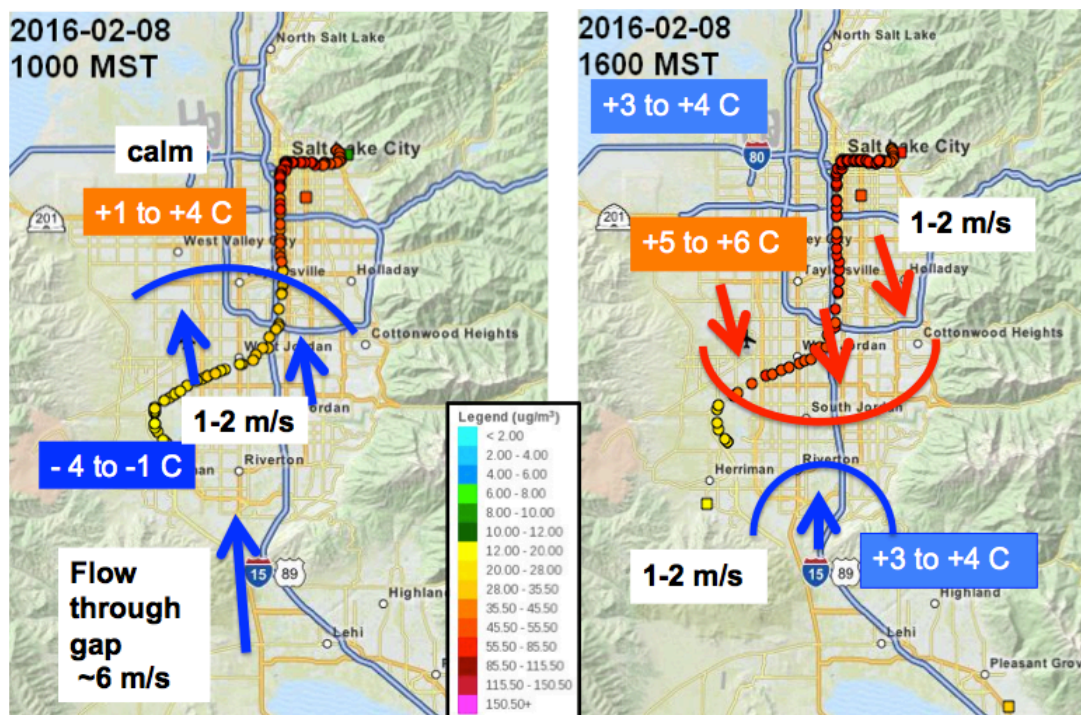
Figure 18: Meteorological analysis of 8 February 2016. Movement of an air mass boundary located in the Salt Lake City controls the PM$_{2.5}$ pollution concentrations as recorded by TRAX-based mobile observations.

A meteorological analysis shows that the PM$_{2.5}$ concentration variations are connected with an air mass boundary. A cold southerly flow is seen that pushes cleaner air to the north, undercutting a warmer, more polluted air mass.

In the afternoon the flow reverses, as the southerly inflow through the Jordan narrows weakens (**Fig 18**). Air with higher PM$_{2.5}$ concentrations is advected southward, degrading the air quality in the central part of the Salt Lake City basin. As the day develops and a convective boundary layer replaces the nocturnal stable boundary layer, pollution is also mixed to higher elevations, and up-valley thermally-driven circulations pump polluted air into the tributary canyons. The concentrations near the mouth of Red Butte Canyon no longer show a minimum in the pollution levels.

Vertical variations

The flight of 9 February 2016 of the KSL news helicopter equipped with a $PM_{2.5}$ monitor is discussed here to illustrate the large vertical variations and the intra-basin spatial variability in $PM_{2.5}$ pollution. **Figure 19** shows the flight summary, projecting the flight-level $PM_{2.5}$ concentrations on a map.
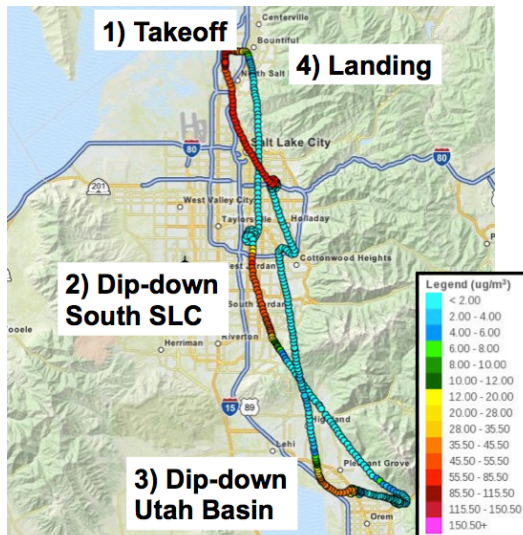
Figure 19: Summary of the 9 February 2016 flight of the KSL new helicopter equipped with a $PM_{2.5}$ sensor. Flight-level concentrations of $PM_{2.5}$ are projected on the map.

In **Figure 20**, the time series of the helicopter flight level and of the measured $PM_{2.5}$ concentrations is shown, color-coded by location or topographic sub-basin. Vertical profiles of $PM_{2.5}$ concentrations can be extracted, representing the various topographic sub-basins as shown in the right panel of **Figure 20**. During 9 February 2016, the surface $PM_{2.5}$ concentrations in the Salt Lake Basin of 55 µg m^{-3} exceeded the concentrations seen in the Utah basin by 15 µg m^{-3}, and the $PM_{2.5}$ pollution layer extended to levels 100 m higher above ground. Note that there is a yet un-quantified uncertainty associated with these airborne $PM_{2.5}$ observations, as the influences of helicopter travel speed and ascent rates on the measurements have not been analyzed.
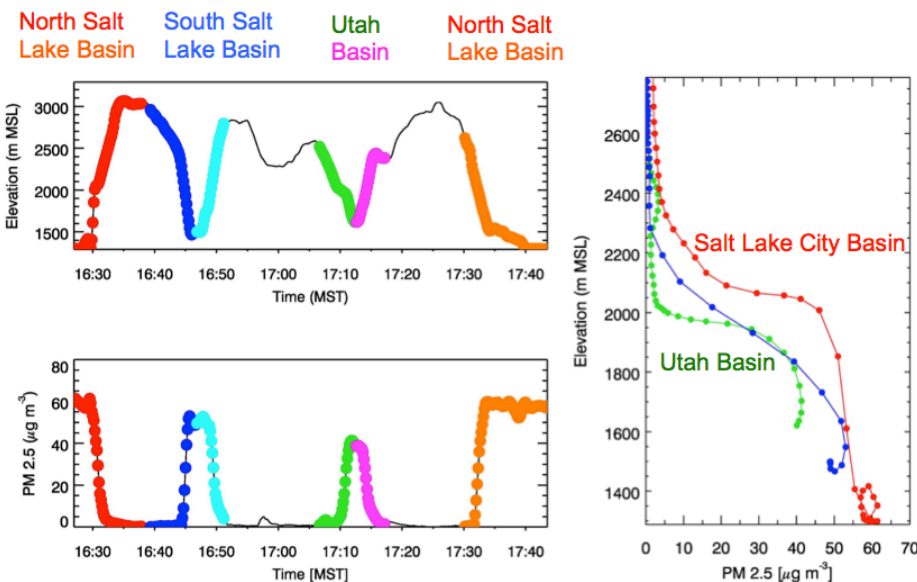
Figure 20: Analysis of the data collected during the helicopter flight of 9 February 2016. On the left hand side, time series of flight level (top) and flight-level $PM_{2.5}$ concentration are shown, color-coded by topographic sub-basin as shown in the legend. On the right hand side, vertical profiles of $PM_{2.5}$ concentrations for three locations are shown, illustrating the spatial variation of the vertical structure of the particulate pollution.

4.2   Evolution of a pollution episode

The last pollution episode of the winter season occurred from 6-16 February 2016. Lasting for 10 days, it was also the longest episode of the season, and it was also the episode with the highest $PM_{2.5}$ concentrations.

Chemical and meteorological conditions during this multi-day episode are examined in greater detail in **Figure 21**. As shown in **Figure 21a**, the $PM_{2.5}$ concentrations exhibit the distinct stages of (a) an initial increase, (b) a period of constant, peak-level concentrations, and (c) a rather quick decrease at the end. Here, the rate of $PM_{2.5}$ increase is about 7 µg m^{-3} day^{-1}, consistent with the range 6-10 µg m^{-3} day^{-1} reported previously (Whiteman et al. 2014, Silcox et al. 2012). The constant peak or "saturation" level is around 60 µg m^{-3}, again matching the climatological average for extended Salt Lake Valley pollution episodes reported by Whiteman et al. (2014). Daily average $PM_{2.5}$ levels exceeded NAAQS for 24-h $PM_{2.5}$ of 35 µg m^{-3} for eight days in a row (7-14 February 2016).

Figure 21b, illustrates the accumulation of NO_x, reaching values as high as 200 ppb and 100 pbb at the valley HW, and basin sidewall UU sites, respectively. Concentrations eventually converged at both sites, indicating a valley-wide buildup of NO_x, as seen in the later stages of the pollution episode. In contrast, peak O_3 and N_2O_5 concentrations, and peak a production rate of NO_3 radicals (P_{NO3}) exhibit a trend opposing NO_x, with a decrease over time (**Fig 21c-d**), consistent with the titration of oxidants by excess NO:

$NO + O_3 \quad \longrightarrow \quad NO_2 + O_2$.
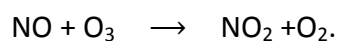
At night, O_3 levels are completely titrated at the HW site, which is rich in NO_x, consistent with a near surface layer with excess NO_x and devoid of oxidants. In contrast, at the higher elevation UU site, O_3 levels as high as 20 ppb are observed at night during the $PM_{2.5}$ buildup period. This indicates favorable condition for nitrate formation. However, after several days, O_3 levels become depleted at the higher elevation, which suggests that oxidant-limited conditions are reaching up to higher elevations. This could be due to a deepening of the cold air pool or strengthening of the cold-air pool capping inversion, reducing the efficient nighttime ventilation and background O_3 import through thermally driven circulations along the sidewall and through tributary canyons. Further, top-down convection in a cloud-topped cold pool can lead to a titration of O_3 as surface NO_x is mixed to layers higher up in the cold air pool.

The production rate of NO_3 radicals, P_{NO3}, via the nighttime reaction

$NO_2 + O_3 \quad \longrightarrow \quad NO_3 + O_2 \quad$ (night),

is shown in **Figure 21d**, where $P_{NO3} = k_2 [O_3][NO_2]$ in units of ppb h^{-1}. Under wintertime, high-NO_x conditions, P_{NO3} is effectively identical to the N_2O_5 production rate via

$NO_3 + NO_2 + M \quad \leftrightarrows \quad N_2O_5$,

as the reduced rate of thermal dissociation of N_2O_5 to NO_3 via

$N_2O_5 + H_2O_{(l)} \quad \longrightarrow \quad 2\ HNO_3$
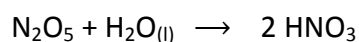
at low temperatures (T < 0°C) shifts the equilibrium between NO_3 and N_2O_5 to strongly favor N_2O_5 (e.g., the $N_2O_5 : NO_3$ ratio is > 300 at 270 K and 10 ppbv NO_2; Chang et al. 2011).
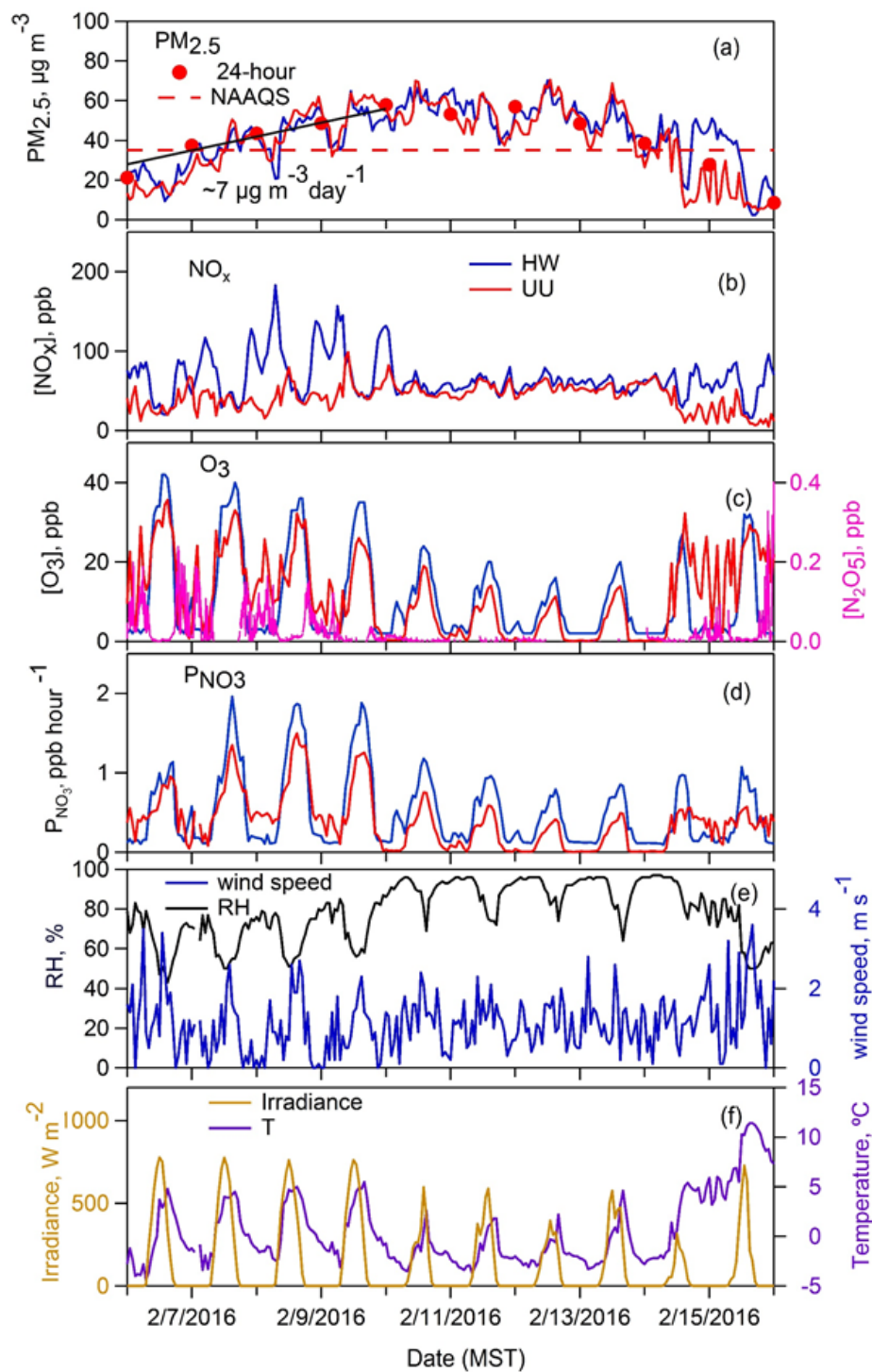
Figure 21: Time series of a) 24-hour and an hourly-averaged PM$_{2.5}$ mass concentration at the UU (red) and HW sites (blue) b) NO$_x$ concentrations, c) O$_3$ and N$_2$O$_5$ concentrations, d) P$_{NO3}$, e) wind speed and relative humidity and f) solar radiation and temperature measured at UU site, for the 6–16 February 2016 pollution episode.

As indicated by pseudo-vertical temperature profiles and time-height cross-sections of ceilometer backscatter, the lower levels of the pollution layer is statically unstable during the day during the build-up phase of the PCAP and vertical mixing occurs until sunset. Therefore the surface measurements made before sunset provide a reasonable approximation for the composition of the residual layer after sunset. The observed decrease in peak P_{NO3} from 2 ppb h^{-1} from the initial stage of pollution increase to < 0.5 ppb h^{-1} at later PCAP stage of high, but stagnating pollution levels, indicate the reduction of the potential for N_2O_5 formation at night. This reduced potential then limits the conversion of NO_x into particulate nitrate via

$$N_2O_5 + H_2O_{(l)} \longrightarrow 2\ HNO_3,$$
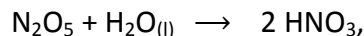
which is the most important heterogeneous reaction in the atmosphere responsible for the removal of NO_x and formation of particulate nitrate (Brown and Stutz 2012, Chang et al. 2011).
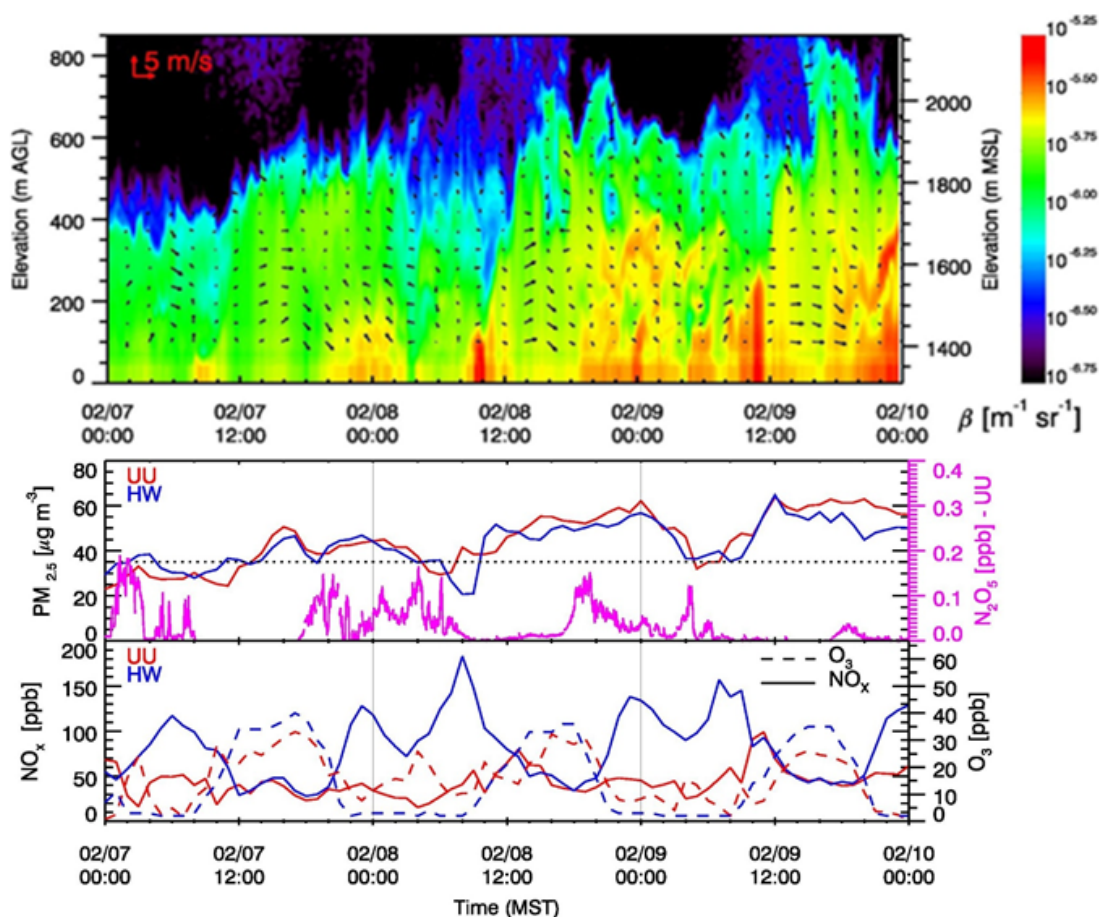
Figure 22: Time-height cross-section of aerosol backscatter at HW during the initial three days of the build-up period of the 6-16 February 2016 pollution episode. Color contours show backscatter coefficient β. The vertical profile of horizontal winds is shown as vectors.

Ceilometer backscatter observations during the first three days of the initial PCAP build-up phase of the 6-16 February event are shown in **Figure 22**, together with time series of $PM_{2.5}$, N_2O_5, NO_x and O_3 concentrations at the HW and UU sites (N_2O_5 only at UU). Several findings are noteworthy. First, ceilometer data shows increases in backscatter at typical times during the diurnal cycle, (a) in the early morning just after sunrise, and (b) during the nighttime hours. Additional peaking occurs regularly after injections of cleaner air during the night are indicated. As shown in **Section 3.2**, aerosol backscatter can be related to concentrations of particulate pollution, but many other factors, such as relative humidity or chemical composition affect this relationship. Nevertheless we think that the increases in backscatter values indicate an increase in concentrations of particulate pollution or *aerosol formation*.

The nighttime increases in backscatter are likely the result of the nighttime chemistry via N_2O_5. The rate of nighttime formation thus depends on the availability of oxidants such as O_3 and the injection of cleaner air with background O_3 via slope and valley flows are enhancing this nighttime chemistry. We further hypothesize that strong morning peaks in aerosol formation are related to rapid processes involving photolabile nighttime radicals reservoirs. In general, photochemical generation of free radicals is weak during wintertime due to reduced solar insolation, low ozone and low absolute water vapor concentrations that combine to significantly reduce OH radical generation from ozone photolysis [Levy 1971]. However, potential radical sources that may drive the early morning chemistry are photolabile nighttime radicals reservoirs, such as $ClNO_2$ and HONO, which are known to form and accumulate over night, and photolyze in the morning (Brown and Stutz 2012, Young et al. 2012). Given the presence of aerosol chloride in Salt Lake Valley (Kelly et al. 2013) and the evidence of N_2O_5 chemistry at night, chlorine activation via heterogeneous chemistry of N_2O_5 could be an important pathway driving the aerosol formation in the early morning hours. As suggested in **Figure 22**, the development of a convective boundary layer near the surface leads to a rapid mixing of the newly formed ammonium nitrate aerosols to upper levels of the PCAP. This vertical mixing is further discussed in **Section 4.3.1**.

4.3   Important Meteorological Processes

In this section, selected meteorological processes are highlighted that influence the temporal and spatial distribution of particulate pollution in the Salt Lake Valley, either by affecting the thermal structure of the PCAP or by affecting the chemical processes.

4.3.1 Sidewall Ventilation

Despite a high VHD observed in the initial days of the 6-16 February pollution episode, daytime heating near the valley floor and vertical mixing is indicated by the ceilometer backscatter

profiles (**Fig. 22**, for example). With the northeastern part of the basin exposed to the early afternoon sun, polluted air from the valley floor rises along the basin sidewall and is ejected into the free atmosphere or into elevated regions of the valley cold pool. A schematic of the process is shown in **Figure 23**.
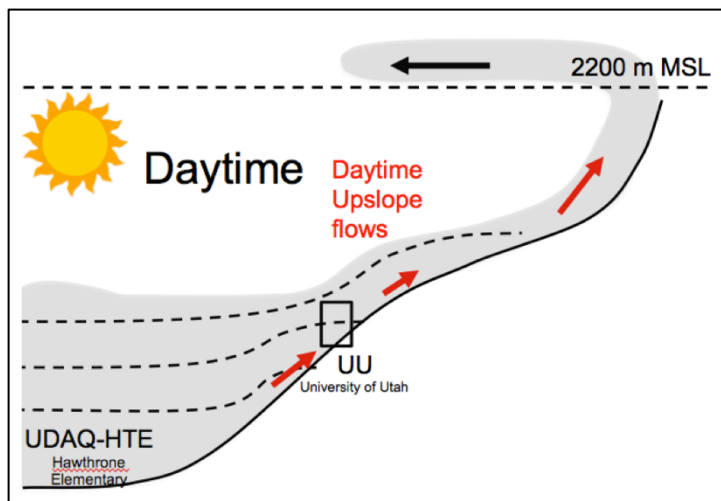
Figure 23: Schematic of the daytime valley sidewall ventilation process along the northeastern benches of the Salt Lake City basin. Polluted air from lower parts of the valley cold pool can be ejected into upper levels, that can be affected by stronger above-basin flows, leading to elevated aerosol layers.

This process is likely responsible for deteriorating air quality at the canyon exit seen in **Figure 18** and discussed in **Section 4.1**. **Figure 24** shows the ceilometer-derived aerosol backscatter, lidar-derived wind profile and σ_w contours for 9 February 2016. This figure illustrates the post-sunrise aerosol formation due to photolabile nighttime radical reservoirs (0900-1100 MST), the onset of convection near the surface, and growth of the convective boundary layer. An elevated aerosol layer can be seen starting at 1500 MST. This aerosol layer is the result of the sidewall ventilation process.
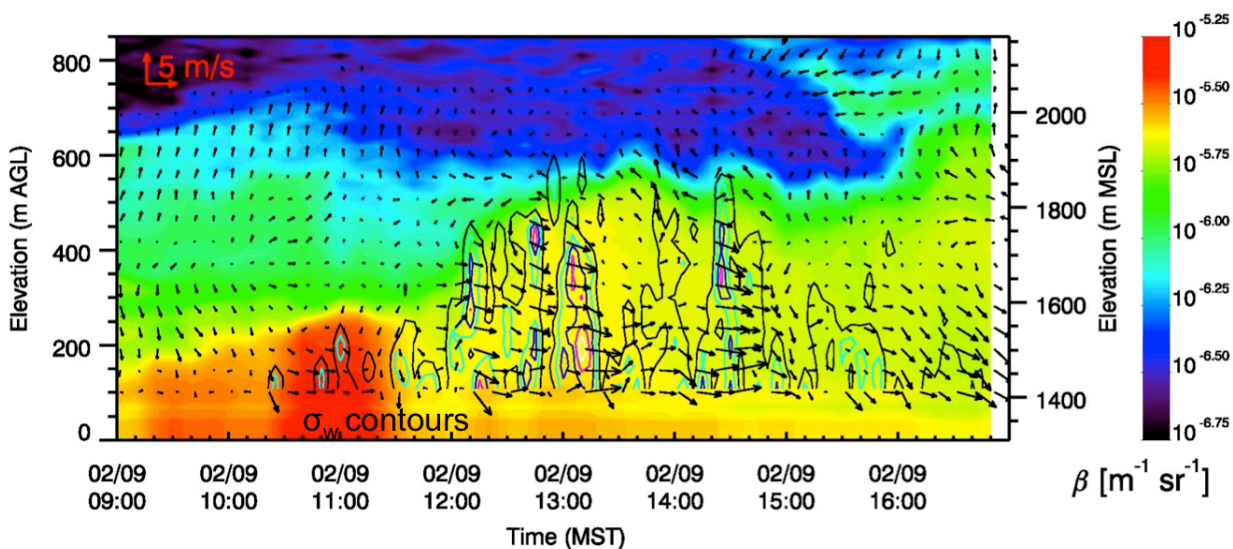
Figure 24: Ceilometer-derived aerosol backscatter, lidar-derived wind profile and σ_w contours from observations at HW on 9 February 2016, illustrating conditions observed above the valley floor consistent with the sidewall ventilation process.

26

4.3.2 Canyon Inflows

Initial findings regarding the chemical processes of aerosol formation indicate the importance of the injection of cleaner, oxidant-rich air into the valley cold-air pool. On the other hand, lower concentrations of particulate pollution are found during the night at the exits of tributary canyons along the Salt Lake Valley.

Figure 25 shows a time series of wind speed, wind direction, and PM$_{2.5}$ concentrations for 3.5 days starting at noon of 6 February 2016, and for selected sites in the Salt Lake Valley. The most striking differences in pollution levels is the strong drop in concentrations at the Red Butte (RB) site located at the mouth of Red Butte Canyon, as illustrated in the small map insert of **Fig. 25**. This drop in PM$_{2.5}$ concentrations coincided with the onset of a nocturnal down-valley circulation, indicated by a persistent down-canyon wind direction (~80°) and elevated wind speeds.
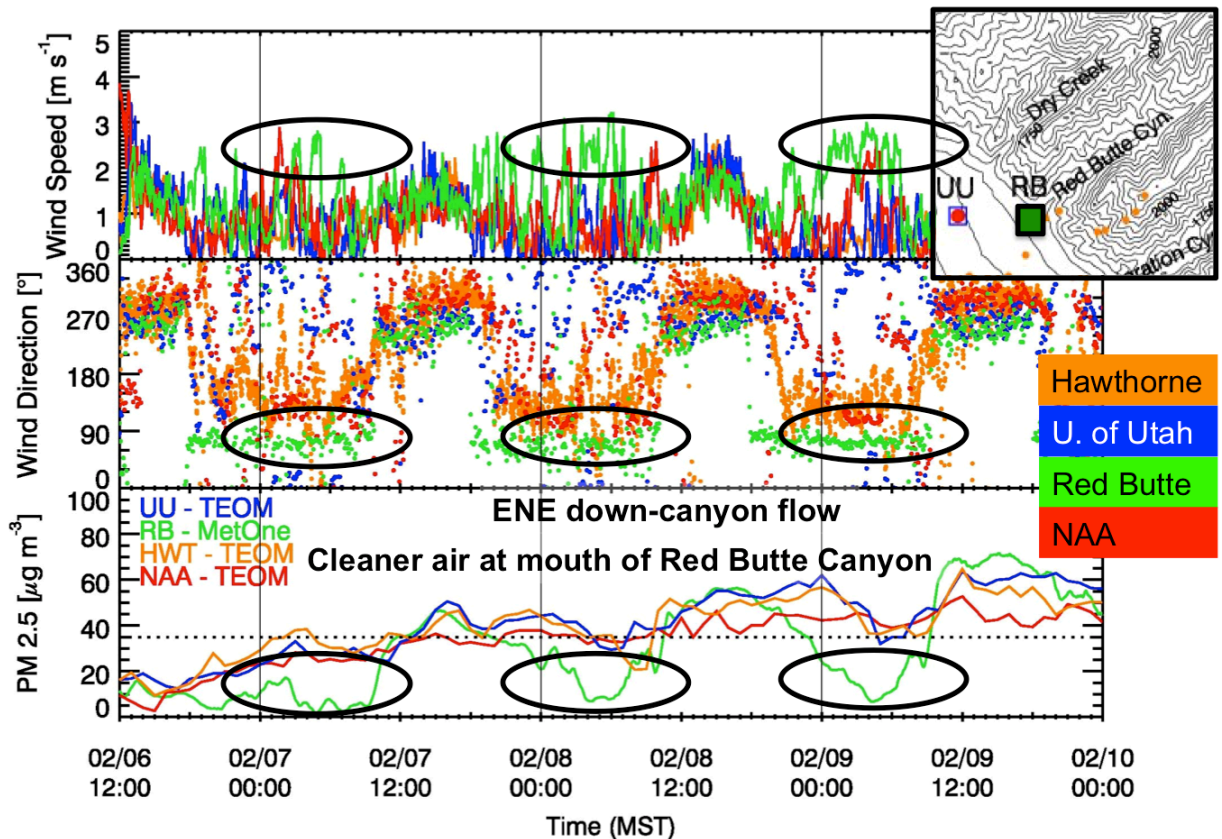
Figure 25: Time series of wind speed, direction, and PM$_{2.5}$ concentrations for 1200 MST 6 Feb 2016 to 0000 MST 10 Feb 2016. A drop in PM$_{2.5}$ concentrations at the RB site is associated with the development of nocturnal down-canyon flows.

The above example shows clear evidence of the strong influence of nocturnal thermally driven circulations on particulate pollution at the mouth of Red Butte Canyon. While this canyon

27

enters the basin at a high elevation on the sidewall, other canyons enter the basin at lower elevations, such as Parleys Canyon or Little Cottonwood Canyon. Parleys Canyon has, besides the entry at a relative low elevation, a much larger air shed, and thus the potential to significantly impact the Salt Lake Valley cold-air pools.

While no observations of pollutant concentrations or aerosol backscatter are available near the month of Parleys Canyon, there are some indications of clean air advection at elevated levels above the HW site, as shown in **Figure 26**. These clean-air injections may originate from down-valley flows within Parleys Canyon or Emigration Canyon.
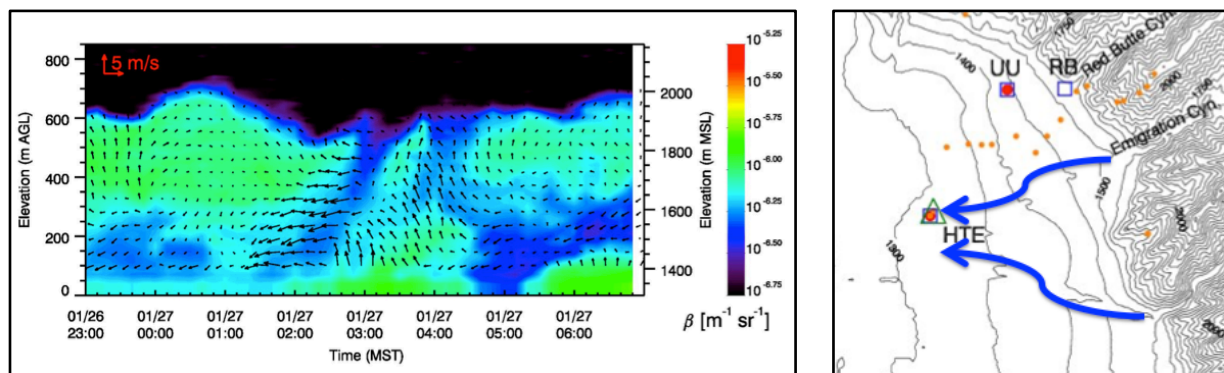
Figure 26:   Ceilometer backscatter and lidar wind field observed at HW in the night of 26-17 January 2016 (left panel). Easterly flow advects cleaner air above the site, which could be due to clean air injections from the deep tributary canyons such as Parleys Canyon or Emigration Canyon, as illustrated in the right panel.

In summary, clean air injections along the valley sidewalls or at levels closer to the valley floor potentially play an important role. On one hand, cleaner air is advected and is associated with a drop in $PM_{2.5}$ concentration. On the other hand, these injections replenish oxidants that are necessary for, and may trigger, additional secondary aerosol formation. To investigate these competing influences, more studies are needed. We hypothesize that the topographic characteristics that control the potential of thermally driven circulations and thus the potential oxidant influx, may control the peak level of $PM_{2.5}$ concentration of the basin that is reached during an extended pollution episode. To test this hypothesis, more observations of both the chemical and meteorological processes in different valleys and basins are necessary.

4.2.3 Additional Meteorological Processes

Other processes have been identified to play an important role in controlling the spatial and temporal variation of $PM_{2.5}$ concentrations in the Salt Lake Valley. These include air mass exchange with the lake boundary layer of the Great Salt Lake related a lake breeze wind system (Crosman and Horel 2016) and mechanical mixing and erosion of the valley cold pool due to high above-basin winds (Lareau and Horel 2015).

5. Online Resources

Visualizations of the various datasets are available for reference and download via the following links:

Overview over basic meteorology and chemical species:

- http://www.inscc.utah.edu/~hoch/DAQSTUD/quicklooks/aws_meteo/

Overview over Lidar-retrieved winds at the HW site:

- http://www.inscc.utah.edu/~hoch/DAQSTUD/quicklooks/lidar_hwt/

Overview over ceilometer-derived aerosol backscatter profiles:

- HW site: http://www.inscc.utah.edu/~hoch/DAQSTUD/quicklooks/ceil_hwt/

- UU site: http://www.inscc.utah.edu/~hoch/DAQSTUD/quicklooks/ceil_wbb/

- RB site: http://www.inscc.utah.edu/~hoch/DAQSTUD/quicklooks/ceil_mtn/

6. Acknowledgements

7. References

Chang, W., Heterogeneous Atmospheric Chemistry, Ambient Measurements, and Model Calculations of N_2O_5: A Review, 2011. *Aerosol Science and Technology*, 45, (6), 665-695. ISSN 0278-6826.

Crosman, E. T. and J. D. Horel, 2016: Winter Lake Breezes near the Great Salt Lake. *Boundary Layer Meteorology*, 159, 2,439-464. DOI: 10.1007/s10546-015-0117-6

Brown, S. S., and J. Stutz, 2012: Nighttime radical observations and chemistry. *Chemical Society Reviews*, 41, (19), 6405-6447. DOI: 10.1039/c2cs35181a.

Fuchs, H., W. P. Dubé, S. J. Ciciora, and S. S. Brown, 2008: Determination of inlet transmission and conversion efficiencies for in situ measurements of the nocturnal nitrogen oxides, NO_3, N_2O_5 and NO_2, via pulsed cavity ring- down spectroscopy. *Analytical Chemistry*, 80, (15), 6010-6017. DOI: 10.1021/ac8007253.

Horel, J., M. Splitt, L. Dunn, J. Pechmann, B. White, C. Ciliberti, S. Lazarus, J. Slemmer, D. Zaff, and J. Burks, 2002: Mesowest: Cooperature mesonets in the western United States. *Bull. Amer. Meteor. Soc.* 83, 211–225. DOI: 10.1175/15200477.

Kelly, K. E. , R. Kotchenruther, R. Kuprov, G.D. Silcox, 2013: Receptor model source attributions for Utahs Salt Lake City airshed and the impacts of wintertime secondary ammonium nitrate and ammonium chloride aerosol, *Journal of the Air & Waste Management Association*, 63, (5), 575-590.

Lareau, N., E. Crosman, C. D. Whiteman, J. D. Horel, S. W. Hoch, W. O. J. Brown, and T. W. Horst, 2013: The Persistent Cold-Air Pool Study. *Bull. Amer. Meteor. Soc.,* 94, 51-63.

Lareau, N., and J. D. Horel, 2015: Dynamically Induced Displacements of a Persistent Cold-Air Pool. *Boundary Layer Meteorology*, 254, 291-315.

Levy, H., 1971: Normal Atmosphere: Large Radical and Formaldehyde Concentrations Predicted. *Science*, 173, 3992, 141-143.

Silcox, G. D., K. E. Kelly, E. T. Crosman, C. D. Whiteman, and B. L. Allen, 2012: Wintertime PM2.5 concentrations in Utah's Salt Lake Valley during persistent, multi-day cold-air pools. *Atmos. Environ.*, 46, 17-24.

Whiteman, C. D., and S. W. Hoch, 2014: Pseudo-vertical temperature profiles in a broad valley from lines of temperature sensors on the sidewalls. *J. Appl. Meteor. Climatol.*, 53 (11), 2430-2437.

Whiteman, C. D., S. W. Hoch, J. D. Horel, and A. Charland, 2014: Relationship between particulate air pollution and meteorological variables in Utah's Salt Lake Valley. *Atmos. Environ.,* 94, 742-753.

Young, C. J., R. A. Washenfelder, J. M. Roberts, L. H. Mielke, H. D. Osthoff, C. Tsai, O. Pikelnaya, J. Stutz, P. R. Veres, A. K. Cochran, T. C. Vandenboer, J. Flynn, N. Grossberg, C. L. Haman, B. Lefer, H. Stark, M. Graus, J. de Gouw, J. B. Gilman, W. C. Kuster, and S. S. Brown, 2012: Vertically resolved measurements of nighttime radical reservoirs in Los Angeles and their contribution to the urban radical budget. *Environmental Science & Technology*, 46 ,20, 10965. DOI: 10.1021/es302206a.